Investigation of structural, dielectric, and magnetic properties of hard and soft mixed ferrite composites

R. K. Kotnala, Shahab Ahmad, Arham S. Ahmed, Jyoti Shah, and Ameer Azam

Citation: J. Appl. Phys. **112**, 054323 (2012); doi: 10.1063/1.4752030
View online: http://dx.doi.org/10.1063/1.4752030
View Table of Contents: http://jap.aip.org/resource/1/JAPIAU/v112/i5
Published by the American Institute of Physics.

Investigation of structural, dielectric, and magnetic properties of hard and soft mixed ferrite composites

R. K. Kotnala,[1] Shahab Ahmad,[1,2] Arham S. Ahmed,[2] Jyoti Shah,[1] and Ameer Azam[2,3,a)]
[1]*National Physical Laboratory, Dr. K. S. Krishnan Road, New Delhi, India*
[2]*Department of Applied Physics, Aligarh Muslim University, Aligarh, India*
[3]*Centre of Nanotechnology, King Abdulaziz University, Jeddah, Saudi Arabia*

(Received 2 May 2012; accepted 9 August 2012; published online 13 September 2012)

Barium ferrite (hard ferrite) and manganese nickel zinc ferrite (soft ferrite) were successfully synthesized by citrate gel combustion technique. They were used to form the composites by mixing them properly in required compositions $(x)BaFe_{12}O_{19}$-$(1-x)Mn_{0.2}Ni_{0.4}Zn_{0.4}Fe_2O_4$ $(0 \leq x \leq 1)$. X-ray diffraction (XRD) and scanning electron microscopy (SEM) were utilized to investigate the different structural and morphological parameters of pure and mixed ferrite composites. XRD and SEM results confirmed the coexistence of both phases in the composite material. Moreover, it has been observed that the composites were constituted by nanosized particles. Structure of pure soft ferrite was found to be cubic and that of pure hard ferrite was hexagonal. Dielectric constant (ε' and ε'') and dielectric loss (tan δ) were analyzed as a function of frequency and composition and the behaviour is explained on the basis of Maxwell-Wagner model. It was observed that the dielectric loss decreases with the increase of hard ferrite content in the composite material. Magnetic measurements suggest the exchange coupling between the magnetizations of soft and hard ferrite grains. It has been observed that the coercivity increases with the increase of the volume of the hard phase in the composite material after an optimal value. © *2012 American Institute of Physics*. [http://dx.doi.org/10.1063/1.4752030]

I. INTRODUCTION

Nanocrystalline ferrites are one of the most attracting classes of materials due to their fascinating applications like transformer core, antenna rod, recording head, loading coil, memory, and microwave devices. Practical applications of ferrites include household, electronics, and computers. Apart from their technological importance in the electronic and magnetic industries, ferrites have been used as a highly reproducible gas[1,2] and humidity[3] sensor material. As ferrites are metal iron oxides, which exhibit properties such as various redox states, electrochemical stability, pseudocapacitive behavior, etc., they can also be used in supercapacitors and in Li-batteries.[4] The properties of ferrite materials are known to be strongly influenced by their composition and microstructure that in turn are sensitive to the processing methods used to synthesize them. Typically, ferrites exhibit two types of structural symmetries, i.e., cubic ferrites and hexagonal ferrites. Cubic ferrites have the general formula MFe_2O_4, where M is a bivalent ion such as Mn^{2+}, Ni^{2+}, Fe^{2+}, Co^{2+}, or Mg^{2+}. All cubic ferrites crystallize in spinel structures that are magnetically soft and easily magnetized and demagnetized.[5,6] Hexagonal ferrites such as $BaFe_{12}O_{19}$ are known to be permanent magnets. Because of their high Curie temperature, very large magnetocrystalline anisotropy, high coercivity, and high magnetization, hexagonal ferrites are used in magnetic recording materials.[7,8] There are many papers reported in literature emphasizing the structural, electrical, and magnetic properties of various soft and hard ferrites. Azadmanjiri has studied the structural and electromagnetic properties of Ni-Zn ferrites prepared by sol-gel combustion method.[9] He found that dielectric constant and dielectric loss decrease with the increase in Zn content. Xu *et al*. have studied the effect of $Ni(OH)_2$ coating on the electromagnetic properties of hexagonal barium ferrite (BaF). They have shown that the $Ni(OH)_2$ coating on the BaF particle surfaces showed no improvement of the complex permeability, while the complex permittivity was greatly enhanced.[10]

To the best of our knowledge, no literature is available on the structural and dielectric properties of mixed hard-soft ferrite composites. In an attempt to prepare high performance ferrites with reproducible stoichiometric compositions and desired microstructure, the present work aimed at synthesis of barium ferrite as a hard ferrite while Mn–Ni–Zn ferrite as a soft ferrite using the sol–gel combustion method and study of structural, dielectric, and magnetic properties of both pure soft and hard ferrites and their composites.

II. EXPERIMENTAL

Both hard ferrite and soft ferrite were prepared by citrate gel technique separately. In the present work, we have chosen barium ferrite $BaFe_{12}O_{19}$ as hard ferrite and manganese nickel zinc ferrite, a representative composition, viz., $Mn_{0.2}Ni_{0.4}Zn_{0.4}Fe_2O_4$ as soft ferrite. The starting materials were barium acetate $(Ba(CH_3COO)_2)$ and iron nitrate $(Fe(NO_3)_3.9H_2O)$ for the synthesis of barium ferrite. Stoichiometric amount of metal salts was dissolved in a minimum amount of distilled water and mixed together thoroughly. Subsequently, $Ba(CH_3COO)_2$ and $Fe(NO_3)_3 \cdot 9H_2O$ solutions

a)Author to whom correspondence should be addressed. Electronic mail: azam222@rediffmail.com. Tel.: +966 531185621. Fax: +966 26951566.

were mixed in citric acid solution drop by drop with constant stirring at room temperature. Previous studies have shown that a 1:1 mole ratio of metal and citric acid is the best ratio for the synthesis of ferrite particles.[10] The homogeneous solution was obtained after mixing the aqueous solutions of the metal salts and citric acid with its natural pH equal to 1. An aqueous solution of ammonia (30%) was then added to increase the pH of the resulting solution up to 9. The solution was slowly evaporated for 24 h at 40 °C to form a viscous gel. Afterwards, the temperature of the hot plate magnetic stirrer was increased up to 160 °C to obtain porous powder of $BaFe_{12}O_{19}$ followed by self combustion. During this process, the gel swells into a fluffy mass.

A similar procedure was adopted for the synthesis of $Mn_{0.2}Ni_{0.4}Zn_{0.4}Fe_2O_4$ powder. The starting materials chosen for synthesis of $Mn_{0.2}Ni_{0.4}Zn_{0.4}Fe_2O_4$ were $Mn(NO_3)_2.4H_2O$, $Zn(NO_3)_2.6H_2O$, $Ni(NO_3)_2.6H_2O$, $Fe(NO_3)_3.9H_2O$, and citric acid ($HOC(CH_2CO_2H)_2{\cdot}CO_2H$). After getting the porous powder of $BaFe_{12}O_{19}$ and $Mn_{0.2}Ni_{0.4}Zn_{0.4}Fe_2O_4$, a heat treatment was done at 1000 °C and 900 °C for 5 h in ambient atmosphere, respectively, to get a pure phase of each ferrite. After final sintering, the materials were ground in mortar for 30 min. These materials were then used to form the composites by mixing them properly in required compositions $(x)BaFe_{12}O_{19}$-$(1-x)Mn_{0.2}Ni_{0.4}Zn_{0.4}Fe_2O_4$ $(0 \leq x \leq 1)$. Total eleven composites were prepared for different values of x varying from 0.0 to 1.0 with an interval of 0.1. Finally, the composite samples were divided into two categories, i.e., in pallets form and in powder form and all of them were then finally annealed at 1100 °C for complete phase formation of the composite.[11] The palletization was done at a pressure of 0.74 MPa. These pallets were used for scanning electron microscopy (SEM) and dielectric measurements while the powdered samples were used for x-ray diffraction (XRD) and magnetic measurements.

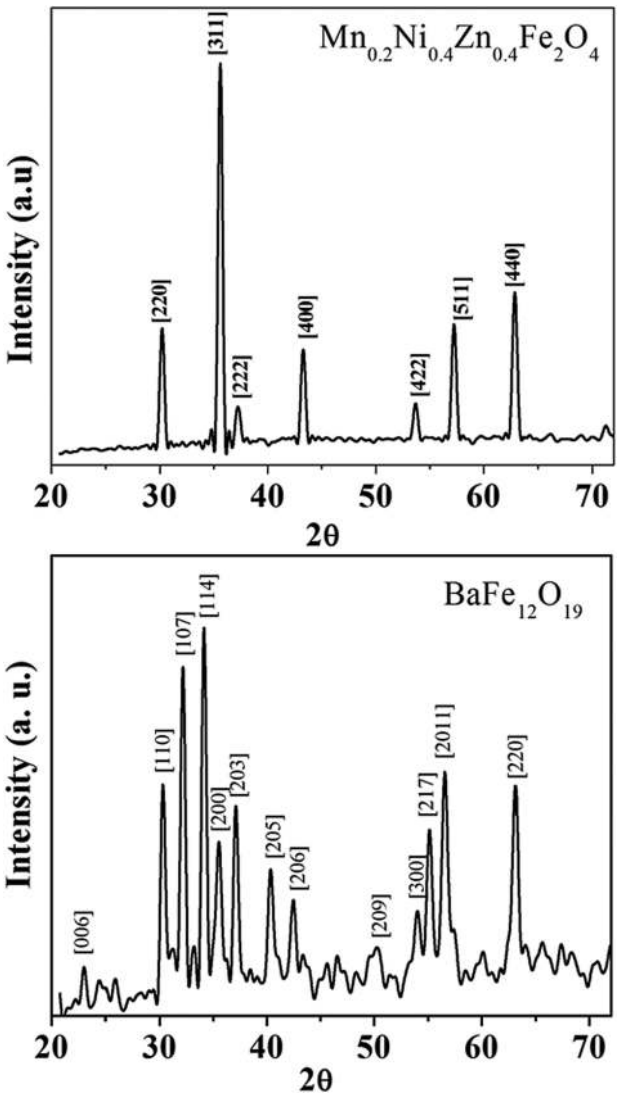

FIG. 1. XRD patterns of the pure ferrites prepared by citrate gel method annealed at 1100 °C.

III. RESULTS AND DISCUSSIONS

A. Structural analysis

Structural properties of barium ferrites and manganese nickel zinc ferrite composites prepared from gel combustion technique were investigated by x-ray diffraction (Rigaku Miniflex II) with Cu Kα radiation of wave length $\lambda = 1.5406$ Å. The scanning range was from 20° to 80° in step size of 0.02 to identify the phase formed and to confirm the completion of the chemical reaction. Figure 1 shows the x-ray diffractograms for manganese nickel zinc ferrite and barium ferrite samples prepared by the citrate gel technique. The lattice parameters were calculated for pure ferrites using Bragg's law. The lattice parameter "*a*" for the soft ferrite (Cubic ferrite) was found out to be 8.3618 Å, while the lattice parameters "*a*" and "*c*" for the hard ferrite (hexagonal ferrite) were found out to be 5.849 Å and 20.976 Å, respectively. Figure 2 shows the XRD pattern for the composites of hard and soft ferrites heated at 1100 °C. The figure clearly shows that the characteristic peaks for both soft ferrite and hard ferrite are present in all the composites having different compositions of soft and hard ferrites. Figure 3 shows the composite at $x = 0.8$ showing coexistence of both phases in the x-ray diffraction pattern. This confirms the existence of the two independent major phases in the composite, without any chemical reaction. No extra peak within the resolution of the XRD technique is detected in all the XRD patterns although the samples have undergone different heating processes. From the XRD pattern of the composites, it is observed that there is no change in the peak positions of the soft ferrites ($Mn_{0.2}Ni_{0.4}Zn_{0.4}Fe_2O_4$) and hard ferrites ($BaFe_{12}O_{19}$). The soft ferrite ($Mn_{0.2}Ni_{0.4}Zn_{0.4}Fe_2O_4$) is showing its characteristics peak at $2\theta = 35.579°$ having the hkl plane at (311). The hard ferrite ($BaFe_{12}O_{19}$) is showing its characteristics peak for the hkl plane at (114) $2\theta = 34.381°$ as shown in figure. Porosity of the samples has been calculated by using

$$\%P = (1 - d_x/d_{\exp}) \times 100, \quad (1)$$

where d_x and d_{exp} are the x-ray density and the experimental density of the samples, respectively.

Morphological studies were carried out using a SEM model LEO 440. In order to avoid the charging problem in

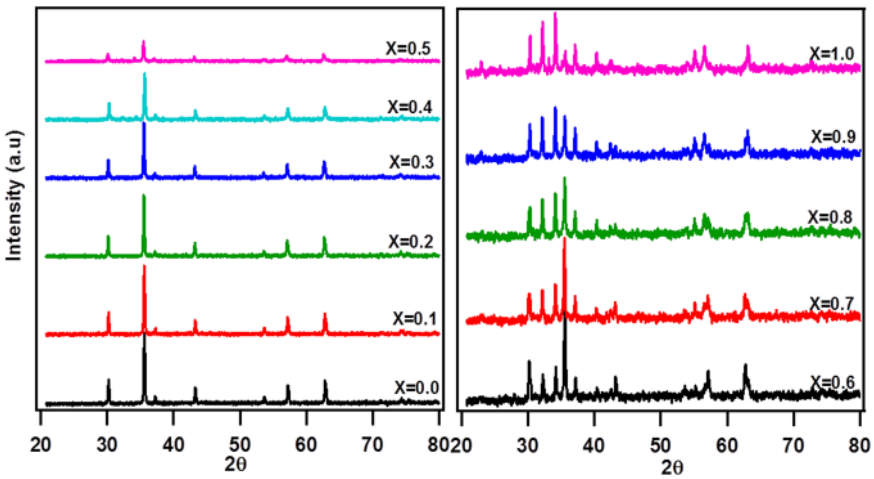

FIG. 2. X-ray diffraction pattern of $(x)BaFe_{12}O_{19}$-$(1-x)Mn_{0.2}Ni_{0.4}Zn_{0.4}Fe_2O_4$ (x = 0–1) composites heated at 1100 °C.

the insulating composite mixture, a very thin layer (8–10 nm) of gold-palladium was coated on the samples. Figure 4 shows SEM images of 100% hard ferrite and 100% soft ferrite which reveal the particle size and morphology of the samples. Figure 4(a) exhibits the SEM image of the pure barium ferrite annealed at 1000 °C showing a presence of small and large grains with poor connectivity in which the ratio between BaF grain size and SF grain size is too large (7:3) to expect any detection of an intergrain exchange interaction. While Figure 4(b) shows that the grain size distribution in pure manganese nickel zinc ferrite annealed at 900 °C is almost uniform with better connectivity. The grain size in pure soft ferrite sample varies from 150 to 350 nm. Porosity of pure barium ferrite and manganese nickel zinc ferrite has been calculated using Eq. (1) was 15.8% and 17.5%, respectively. From Figure 5, it is also clear that soft ferrite is more porous than hard ferrite. Figure 5(a) corresponds to the SEM image of the composite of soft and hard ferrites with the composition of 20% hard and 80% soft ferrite heated at 1100 °C. The image shows the presence of bigger and smaller particles suggesting that the coexistence of both phases. 17.7% porosity has been observed for this composition. The hard ferrite grains are distributed uniformly over the whole volume and seem to be adsorbed on the surface of the soft ferrite particles in the composite. Figure 5(b) corresponds to the composite having 80% hard and 20% soft ferrite heated at 1100 °C. With increased percent of hard ferrite porosity of the composite decreased to 16.2%. The hard ferrite particles are distributed uniformly and they had surrounded by the soft ferrite particles completely forming a good composite system good connectivity among grains. Figure 6 corresponds to the composite with 50% hard and 50% soft ferrite. It is clear from the figure that both the phases are distributed uniformly and the composite system is having less porosity. As individual ferrite has been annealed at lower temperatures, i.e., barium ferrite at 1000 °C and manganese nickel zinc ferrite at 900 °C, as compared to the annealing temperature of composite which is 1100 °C, there is some increase in average size of grains of both ferrites in the composite system. The porosity of this composite has been determined, 16.8%. This large grains size is basically responsible for the better inter-grain connectivity and less porosity in the composite.

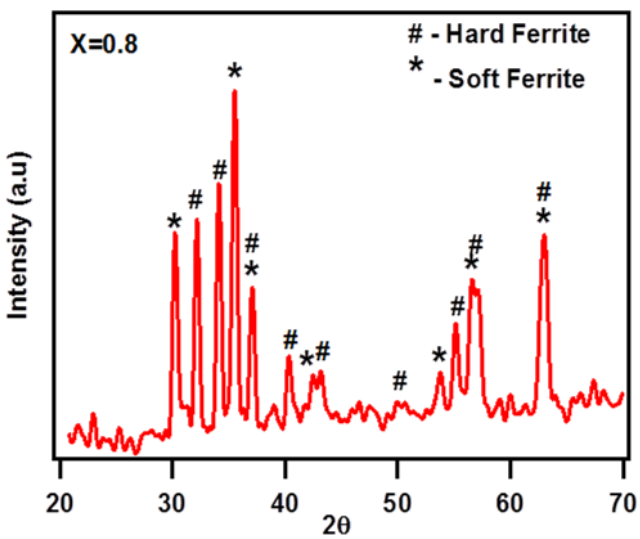

FIG. 3. X-ray diffraction pattern of $(x)BaFe_{12}O_{19}$-$(1-x)Mn_{0.2}Ni_{0.4}Zn_{0.4}Fe_2O_4$ (x = 0–1) composite at x = 0.8 showing co-existence of both hard and soft phases.

B. Dielectric properties

The dielectric measurements were carried out in the frequency range 100 Hz to 10 MHz using Wayne Kerr 6540 A impedance analyser at room temperature. The samples were pressed into circular disc shaped pellets, and silver coating was done on adjacent faces to make the parallel plate capacitor geometry with ferrite material as the dielectric medium. Figs. 7 and 8 show the variation of real and imaginary parts of the dielectric constant of all the composites of $(x)BaFe_{12}O_{19}$-$(1-x)Mn_{0.2}Ni_{0.4}Zn_{0.4}Fe_2O_4$ $(0 \le x \le 1)$, including individual ferrite samples with frequency (1 KHz–10 MHz) at room temperature. It can be observed that all the compositions exhibit dielectric dispersion where both real and imaginary dielectric constants decrease with increasing frequency in low-frequency region while it approaches almost frequency independent behaviour in high frequency region. The decrease in imaginary part of dielectric constant is pronounced more in comparison to real dielectric constant.

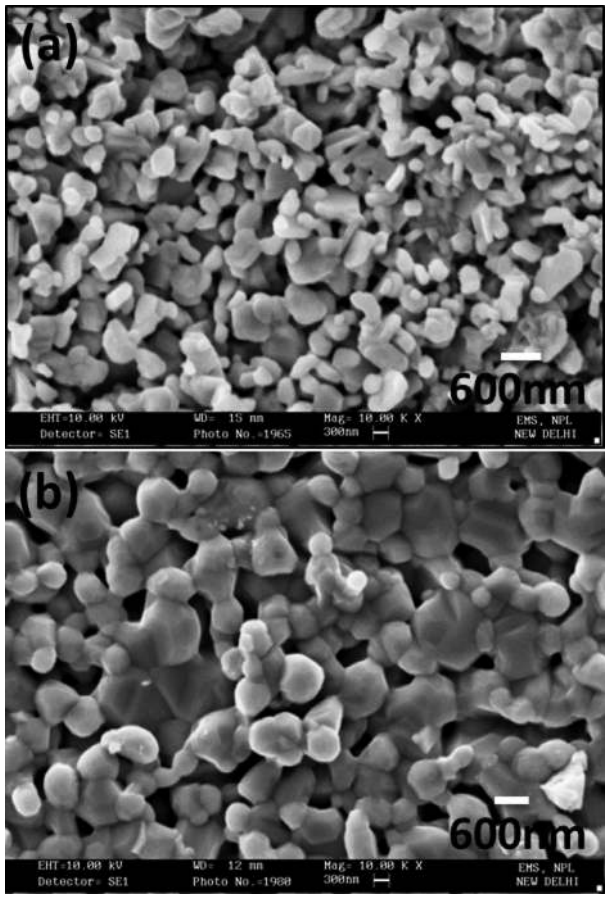

FIG. 4. SEM images of (a) barium ferrites $BaFe_{12}O_{19}$ annealed at 1000 °C and (b) manganese nickel zinc ferrite $Mn_{0.2}Ni_{0.4}Zn_{0.4}Fe_2O_4$ annealed at 900 °C.

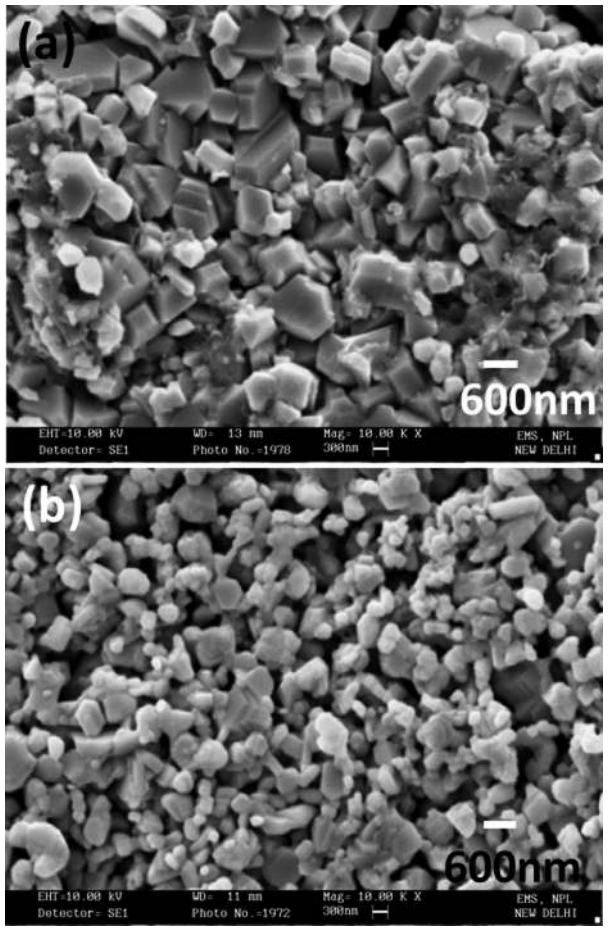

FIG. 5. SEM images of composites of mixture (a) 1:4 ($BaFe_{12}O_{19}$:$Mn_{0.2}Ni_{0.4}Zn_{0.4}Fe_2O_4$) and (b) 4:1 ($BaFe_{12}O_{19}$:$Mn_{0.2}Ni_{0.4}Zn_{0.4}Fe_2O_4$) heated at 1100 °C showing the morphology.

The dielectric dispersion curve can be explained on the basis of Koops's theory,[11] based on the Maxwell–Wagner model for the in-homogeneous double structure.[12] According to this model, the dielectric structure was supposed to be composed of the double layer. The first layer is of fairly well conducting materials, which is separated by the second thin layer (grain boundaries) of relatively poor conducting substance. The grain boundaries were found to be more effective at lower frequencies while the ferrite grains are more effective at higher frequencies. The existence of majority Fe^{3+} ions and minority Fe^{2+} ions has rendered ferrite materials dipolar. However, in an ultrafine regime, both grain boundaries and grains are large in number as compared to the bulk case, which makes the phenomena more complex. Also in nanomaterials, there is an additional chance of having a high dielectric constant because of large surface polarization owing to the large surface area of individual grains. In a low-frequency regime, surface polarization plays a dominant role than electronic or ionic polarization in determining the dielectric properties of ferrite materials.[11] In our measurements, ε' is large, of the order of 10^4, in pure soft ferrite and it starts decreasing by adding hard ferrite in soft ferrite. The decrease in dielectric constant value with increasing frequency is a normal behaviour observed in most of the ferromagnetic materials. The polarization in ferrites is through a mechanism similar to the conduction process. By electron exchange between Fe^{2+} and Fe^{3+}, the local displacement of electrons in the direction of the applied field occurs and these electrons determine the polarization. The observed decrease in dielectric constant with increasing frequency is attributed to the fact that the space charge carriers in a dielectric require a finite time to line up their axes in the direction of an applied alternating field. If the frequency of the field reversal increases, a point reaches when the space charge carriers cannot align with the applied field and does not follow the alternation of the field[13] resulting the decrease in the dielectric constant of the material. As the frequency of the field continues to increase, at some stage, the space charge polarization will barely have started to move before the field reverses and makes virtually no contribution to the polarization and hence to the dielectric constant of the material. The large value of dielectric constant at lower frequency is due to the predominance of species like Fe^{2+} ions, oxygen vacancies, grain boundary defects, etc., while the decrease in dielectric constant with frequency is natural because of the fact that any species contributing to polarizability is found to show lagging behind the applied field at higher and higher frequencies.[14]

Fig. 9 shows the variation of dielectric loss as a function of frequency (100 Hz to 1 MHz) at room temperature. The dielectric loss gives the loss of energy from the applied field

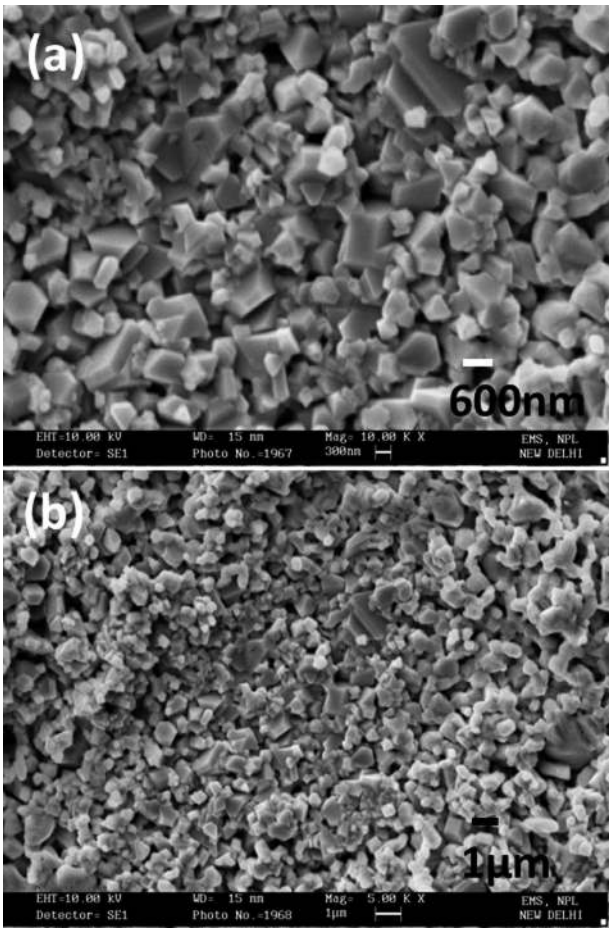

FIG. 6. SEM image of composite having equal ratio of soft and hard ferrite at (a) 10 K X and (b) 5 K X.

into the sample. This is caused by domain wall resonance. At higher frequencies, the losses are found to be low, since domain wall motion is inhibited and magnetization is forced to change rotation. There is a strong correlation between the conduction mechanism and the dielectric behaviour of ferrites.[15] From Fig. 9, it is apparent that dielectric loss for composites at x = 0.0, 0.1, and 0.2 shows the peaking nature

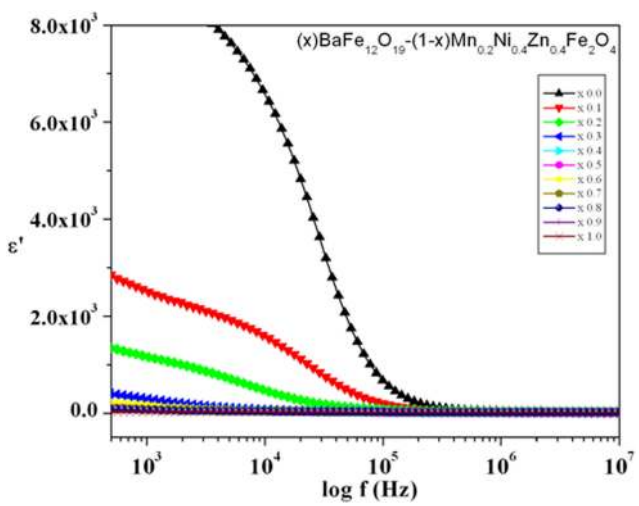

FIG. 7. Variation of real part of dielectric constant of $(x)BaFe_{12}O_{19}$-$(1-x)Mn_{0.2}Ni_{0.4}Zn_{0.4}Fe_2O_4$ $(0 \leq x \leq 1)$ as a function of frequency.

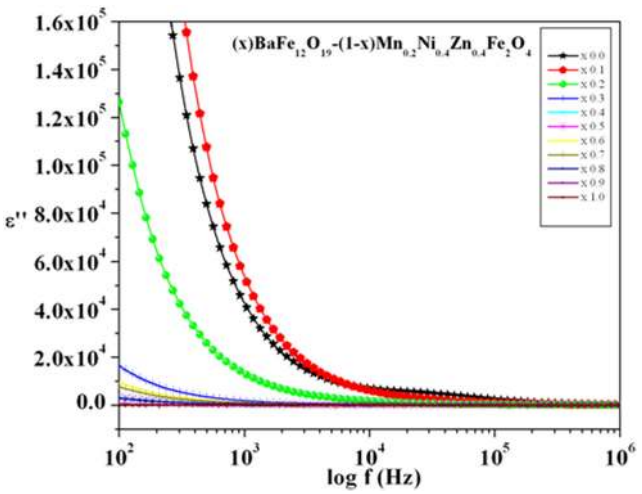

FIG. 8. Variation of imaginary part of dielectric constant of $(x)BaFe_{12}O_{19}$-$(1-x)Mn_{0.2}Ni_{0.4}Zn_{0.4}Fe_2O_4$ $(0 \leq x \leq 1)$ as a function of frequency.

and a slight shift in these maxima is observed. It is also noted that the height of the peak decreases with increasing hard ferrite in soft ferrite and the maxima shift towards lower frequency region. The condition for having maxima in the dielectric losses of a dielectric material is given by the relation (2).

$$\omega\tau = 1, \tag{2}$$

where $\omega = 2\pi f_{max}$ and τ is the relaxation time.

A relation relates the relaxation time to the jumping probability per unit time, p (2) and (3):

$$\tau = 1/2p \tag{3}$$

or

$$f_{max} \propto p. \tag{4}$$

Therefore, from the above relation it is clear that, maxima can be observed when the jumping or hoping frequency of

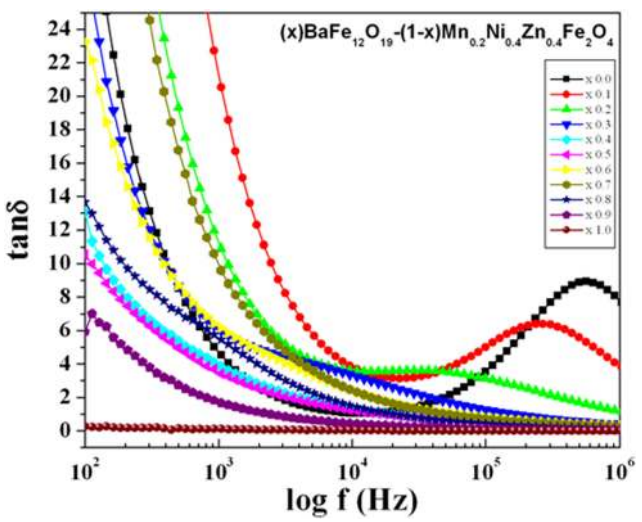

FIG. 9. Variation of loss tangent of $(x)BaFe_{12}O_{19}$-$(1-x)Mn_{0.2}Ni_{0.4}Zn_{0.4}Fe_2O_4$ $(0 \leq x \geq 1)$ as a function of frequency.

electrons between Fe^{2+} and Fe^{3+} becomes approximately equal to the frequency of the applied field.[16]

C. Magnetic properties

Magnetic measurements were carried out using vibrating sample magnetometer (VSM) Lake Shore 7400 series at room temperature. The magnetic properties such as saturation magnetization (M_s), coercivity (H_c), and remanence (M_r) were calculated from the magnetic hysteresis loops. Figures 10(a)–10(k) represent the magnetization versus applied field (M-H) curves of the individual and composite ferrite samples having different values of x in $(x)BaFe_{12}O_{19}$-$(1-x)$ $Mn_{0.2}Ni_{0.4}Zn_{0.4}Fe_2O_4$ $(0 \leq x \geq 1)$.

It is clear from the figures that saturation magnetisation Ms varies between 30 and 50 emu/g, which makes a variation of 70%. It is seen from Fig. 10 that crystallographically two-phased composites show a good single-phase magnetic behaviour suggesting that the magnetic hard and soft phases are exchange coupled in these composites, though the magnetic coupling between these two phases is not well efficient due to size irregularity and large size ratio of hard and soft ferrite grains. Hence, the characteristic behaviour of coercivity maxima (exchange spring behaviour) at certain

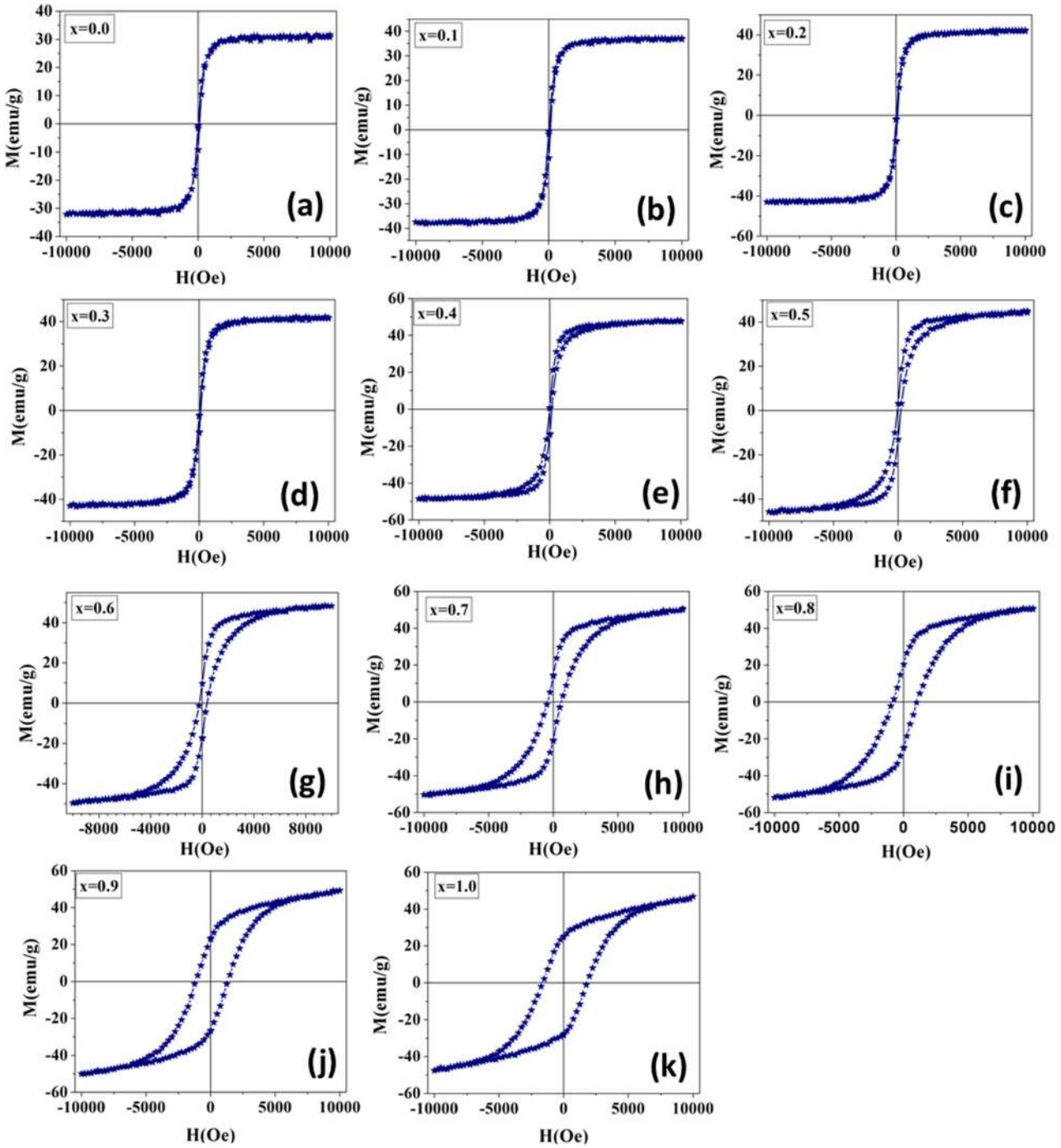

FIG. 10. M-H loops of all the composites of soft ($Mn_{0.2}Ni_{0.4}Zn_{0.4}Fe_2O_4$) and hard ($BaFe_{12}O_{19}$) ferrites annealed at 1100 °C.

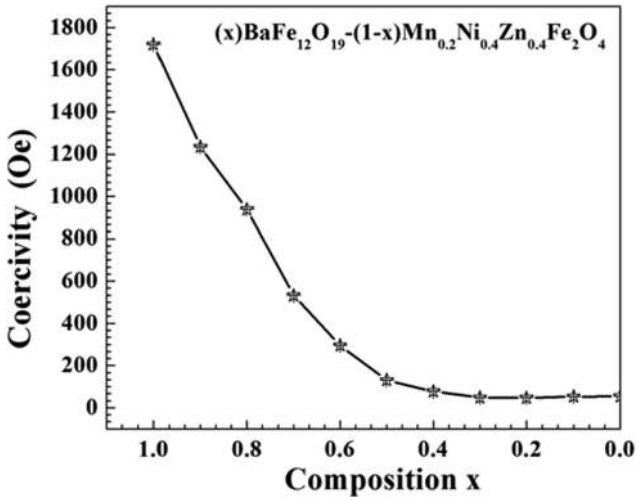

FIG. 11. Variation of the coercivity of the composite heated at 1100 °C with composition "x."

composition of hard/soft ferrite phase has not been observed in this hard/soft ferrite based composite system. If it is not exchange coupled, then the magnetization could have been shown as the superimposition of two loops corresponding to the soft and the hard ferrites instead of a single one. Actually, the magnetic properties of the two-phase composite materials depend very much on the distribution of the magnetically soft and hard phases, the average grain sizes of the individual phases, grain size ratio of hard and soft ferrite phases, the particle shape, etc.[17] For isotropic two-phase magnet, the small grain size improves both remanence and coercivity.[18] In addition to this, there are two main interactions, exchange and dipolar interactions that determine the magnetic property of the two-phase permanent magnet. Since the composite is a mixture of soft and hard phases, there are three exchange energy terms that need to be taken into account, like exchange energy between the soft and the hard (which is dominating), then between soft and soft, and then between hard and hard. If the dipolar interaction is neglected, magnetization in the remanence state is mainly determined by the exchange interaction and magnetocrystalline anisotropy. The hard barium ferrite phase is having large anisotropy; therefore, it is difficult to achieve magnetization reversal with the lower applied field. However, the magnetizations in the soft ferrite grains in the composite are mainly determined by the exchange interaction between the hard and the soft phases due to smaller magnetocrystalline anisotropy of the soft manganese nickel–zinc ferrite. So magnetization of soft grains will be sufficiently exchange coupled with the neighbouring hard grains magnetization. This soft and hard exchange interaction will try to align magnetization in the soft grain. However, an intergrain exchange interaction may not prevail in this case due to large ratio between barium ferrite grain size and manganese nickel–zinc ferrite grain size. But if one considers the dipolar interaction as well, then magnetization distribution of soft grains is the result of competition between the hard and the soft exchange coupling and dipolar interaction.[19]

It can also be seen from the hysteresis loops of the composites at $x = 0.0$, 0.1, 0.2, and 0.3 (Figs. 10(a)–10(d), respectively) that the values of coercivity are very small and it starts increasing for the composites at $x = 0.4$ to 1.0 (Figs. 10(e) to 10(k)). With the increase in volume fraction of the hard barium ferrite phase, the exchange force acting on magnetization in a soft grain of manganese nickel–zinc ferrite becomes strong preventing the magnetization in soft grains from reversal with the reversal of the applied field. In this region, however, the coupling between magnetization inside different hard grains is not very strong, because direct coupling is prevented by the presence of the soft grain and the indirect coupling through soft grains is prevented by small value of soft–soft exchange constant.[20] So the coercivity increases with the increase of the volume of the hard phase after an optimal value as shown in Fig. 11.

IV. CONCLUSIONS

We have successfully synthesized barium ferrite (hard ferrite) and manganese nickel zinc ferrite (soft ferrite) using citrate gel combustion route. XRD spectra confirmed the cubic structure of soft ferrite with the lattice parameter $a = 8.3618$ Å and hexagonal structure of hard ferrite with the lattice parameters $a = 5.849$ Å, $c = 20.976$ Å. XRD patterns of mixed ferrites exhibited the characteristic peaks of both soft ferrite and hard ferrite showing the coexistence of both the phases in composite material. No extra peak was observed in XRD spectra of composite material. Furthermore, there is no change in peak positions of soft and hard ferrites for all the compositions. It has been found from SEM results that soft ferrite is more porous than that of hard ferrite. SEM images of composite material consist of both larger and smaller grains which also confirm the coexistence of both the phases in the composite. It has also been observed that both the phases are distributed uniformly and having less porosity for the composition of 50% soft and 50% hard ferrite. Dielectric constant was found to be maximum for pure soft ferrite and decreases with the increase of hard ferrite in the composite material. Dielectric loss shows the peaking behaviour for the composition of $x = 0.0$, 0.1, and 0.2 and peak maxima decrease with the increase of hard ferrite in soft ferrite. Dielectric loss approaches to zero in case of pure hard ferrite. Magnetic measurements suggest the exchange coupling between the magnetizations of soft and hard ferrite grains, but it is not efficient to exhibit the exchange spring behaviour of coercivity. It has been observed that the coercivity increases with the increase of the volume of the hard phase in the composite material after an optimal value. Therefore, the magnetic properties can be tuned by mixing the soft and hard ferrites for desired applications.

[1]C. V. Gopal Reddy, S. V. Manorama, and V. J. Rao, Sens. Actuators B **55**, 90 (1990).
[2]C. V. Gopal Reddy, S. V. Manorama, and V. J. Rao, J. Mater. Sci. Lett. **19**, 775 (2000).
[3]G. R. Dube and V. S. Darshane, J. Mol. Catal. **79**, 285 (1993).
[4]Y. N. Nuli and Q. Z. Qin, J. Power Sources **142**, 292 (2005).
[5]A. A. Novakova, V. Y. Lanchinskaya, A. V. Volkov, T. S. Gendler, T. Y. Kiseleva, M. A. Moskvina, and S. B. Zezin, J. Magn. Magn. Mater. **258/259**, 354 (2003).

[6]C. R. Vestal and Z. J. Chang, Chem. Mater. **14**, 3817 (2002).
[7]H. F. Yu and K. C. Huang, J. Magn. Magn. Mater. **260**, 455 (2003).
[8]L. Fu, X. Liu, Y. Zhang, V. P. Dravid, and C. A. Mirkin, Nano Lett. **3**, 757 (2003).
[9]J. Azadmanjiri, Mater. Chem. Phys. **109**, 109 (2008).
[10]P. Xu, X. J. Han, X. H. Wang, C. Wang, H. T. Zhao, and W. J. Zhang, Mater. Chem. Phys. **108**, 196 (2008).
[11]C. G. Koops, Phys. Rev. **83**, 121 (1951).
[12]T. Prodromakis and C. Papavassiliou, Appl. Surf. Sci. **255**, 6989 (2009).
[13]V. R. K. Murthy and J. Sobhanadri, Phys. Status Solidi A **36**, K133 (1976).
[14]J. C. Maxwell, *Electric and Magnetism* (Oxford University Press, New York, 1973), p. 828.
[15]K. Iwachi and Y. Ikeda, Phys. Status Solidi A **93**, 309 (1986).
[16]M. A. Dar, K. M. Batoo, V. Verma, W. A. Siddiqui, and R. K. Kotnala, J. Alloys Compd. **493**, 553 (2010).
[17]J. E. Davies, O. Hellwiga, and E. E. Fullerton, Appl. Phys. Lett. **86**, 262503 (2005).
[18]T. Schrefl, J. Fidler, and H. Kronmuller, Phys. Rev. B **49**, 6100 (1994).
[19]D. Roy, C. Shivakumara, and P. S. Anil Kumar, J. Magn. Magn. Mater. **321**, L11–L14 (2009).
[20]H. Fukunaga, J. Kuma, and Y. Kanai, IEEE Trans. Magn. **35**, 3235 (1999).